Taylor & Francis
Taylor & Francis Group

RESEARCH ARTICLE

OPEN ACCESS Check for updates

OCTN2-targeted nanoparticles for oral delivery of paclitaxel: differential impact of the polyethylene glycol linker size on drug delivery *in vitro*, *in situ*, and *in vivo*

Longfa Kou[a], Rui Sun[a,b], Shuyi Xiao[a], Xiao Cui[a], Jin Sun[c], Vadivel Ganapathy[d], Qing Yao[b] and Ruijie Chen[a]

[a]Department of Pharmacy, The Second Affiliated Hospital and Yuying Children's Hospital of Wenzhou Medical University, Wenzhou, China; [b]School of Pharmaceutical Sciences, Wenzhou Medical University, Wenzhou, China; [c]Department of Pharmaceutics, Wuya College of Innovation, Shenyang Pharmaceutical University, Shenyang, China; [d]Department of Cell Biology and Biochemistry, School of Medicine, Texas Tech University Health Sciences Center, Lubbock, TX, USA

ABSTRACT

Targeted nanocarriers have shown great promise in drug delivery because of optimized drug behavior and improved therapeutic efficacy. How to improve the targeting efficiency of nanocarriers for the maximum possible drug delivery is a critical issue. Here we developed L-carnitine-conjugated nanoparticles targeting the carnitine transporter OCTN2 on enterocytes for improved oral absorption. As a variable, we introduced various lengths of the polyethylene glycol linker (0, 500, 1000, and 2000) between the nanoparticle surface and the ligand (CNP, C5NP, C10NP and C20NP) to improve the ligand flexibility, and consequently for more efficient interaction with the transporter, to enhance the oral delivery of the cargo load into cells. An increased absorption was observed in cellular uptake *in vitro* and in intestinal perfusion assay *in situ* when the polyethylene glycol was introduced to link L-carnitine to the nanoparticles; the highest absorption was achieved with C10NP. In contrast, the linker decreased the absorption efficiency *in vivo*. As the presence or absence of the mucus layer was the primary difference between *in vitro*/*in situ* versus *in vivo*, the presence of this layer was the likely reason for this differential effect. In summary, the size of the polyethylene glycol linker improved the absorption *in vitro* and *in situ*, but interfered with the absorption *in vivo*. Even though this strategy of increasing the ligand flexibility with the variable size of the polyethylene glycol failed to increase oral absorption *in vivo*, this approach is likely to be useful for enhanced cellular uptake following intravenous administration of the nanocarriers.

1. Introduction

Nanoparticles have attracted a lot of attention in recent years as drug delivery vehicles to decrease side effects and enhance therapeutic index (Yao et al., 2017b; Regina-Veronicka et al., 2018; Qing et al., 2018). These nanoparticles have shown various advantages for drug delivery, such as increasing the solubility and stability of drugs, improved drug half-life in circulation, optimized drug distribution, and targeted drug delivery. With the recent developments in cell biology and biochemistry, a large number of cell-surface receptors and transporters have been identified and characterized as the molecular targets for these nanoparticles (Kennedy et al., 2002; International Transporter Consortium, 2010; Howard et al., 2014; Kou et al., 2018a; Hu et al., 2019). The target specificity is dictated by the nature of the ligand engineered onto the surface of the nanoparticles. Nanoparticles designed with specific ligands on their surface could target a given receptor or transporter that are

expressed differentially on target cells. This strategy allows drug delivery to a particular tissue or cell type as needed for the treatment of a specific disease (Kou et al., 2017c; Wang et al., 2017; Kou et al., 2018a,b; 2019).

As for the targeted nano-drug delivery systems, many factors are relevant to their targeting efficiency, such as the affinity of the ligand to the molecular target on the targeted cell surface (Kharya et al., 2013; Luo et al., 2016), ligand density (Chu et al., 2016; Li et al., 2017), flexibility of the carrier and the ligand (Kou et al., 2017a), ligand conformation (Chacko et al., 2012), etc. Considerable efforts have been made to analyze quantitatively the influence of these different factors for the maximum possible efficiency of these nano-drug delivery systems. With ligand density as an example, some investigators reported that increased ligand density could result in an increased uptake, indicating an improved targeting efficiency (Shao et al., 2014; Li et al., 2017). There are also some studies showing increased ligand density causing decreased targeting efficiency (Chu et al.,

CONTACT Qing Yao ✉ yqpharm@163.com 🏢 Wenzhou Medical University, University Town, Wenzhou 325035, China; Ruijie Chen ✉ crjpharm@163.com
🏢 109 Xueyuan West Road, Wenzhou 325027, China
⊕ Supplemental data for this article can be accessed here.

2016; Kou et al., 2017b). It was surmised that there is an optimal ligand density for maximal effect; increasing or decreasing the ligand density from this optimal level could interfere with the interaction of nanoparticles with the intended molecular target. In this study, we examined the influence of ligand flexibility on the targeting efficiency of nanoparticles.

Due to issues related to patient satisfaction and compliance, oral administration remains the preferred route of drug delivery for most patients. However, many pharmacological agents have low bioavailability due to their low solubility in aqueous medium, low stability and poor permeability across biological membranes. Nano-drug delivery system could significantly improve their solubility and stability because the drugs are encapsulated within vehicles and at the same time enhance the permeability across the plasma membrane of the enterocytes via endocytosis (Kou et al., 2013). In most instances, targeted nano-drug delivery systems display improved performance in terms of therapeutic efficacy (Date et al., 2016; Yao et al., 2017a,c, 2019). We have recently developed L-carnitine-conjugated nanoparticles to target the carnitine transporter OCTN2 expressed on the enterocytes for enhanced oral bioavailability (Kou et al., 2017a). However, in that initial study, the ligand L-carnitine was directly anchored onto the nanoparticle surface, which might restrict the flexibility and mobility of ligand, resulting in less than desired efficiency in the interaction between the ligand and the transporter. To address this issue specifically, we undertook the present study in which we examined the impact of a polyethylene glycol (PEG) linker between the ligand and the surface of the nanoparticles on oral bioavailability of the drug cargo. We used three different experimental approaches: *in vitro* studies with cultured cells, *in situ* studies with intestinal loop perfusion, and *in vivo* studies with whole animals. We chose PEG because it is hydrophilic, which has been shown to increase the permeability of nanoparticles across the mucus layer at the surface of the intestinal lumen (Song et al., 2018). PEG500, PEG1000 and PEG2000 were selected to test the effects of linker length on the performance of L-carnitine-conjugated nanoparticles (C5NP, C10NP and C20NP).

2. Materials and methods

2.1. Materials

Paclitaxel (PTX) was purchased from Chongqing Meilian Pharmaceutical Co. Ltd. (Chongqing, China). Poly(lactic-co-glycolic acid) (PLGA; PLA:PGA = 50:50; 38,000 MW) was purchased from Jinan Daigang Biological Engineering Co. Ltd. (Jinan, China). Poly(vinylalcohol) (PVA; 20,000–30,000 MW) was sourced from Acros Organics (New Jersey, USA). Methyl thiazolyl tetrazolium, Methylthiazolyldiphenyl-tetrazolium bromide (MTT), L-carnitine, polyoxyethylene stearate ($n = 10$, 25, 40) were purchased from Aladdin biochemical technology Co. Ltd. (Shanghai, China). All other chemicals were from Sigma-Aldrich (Shanghai, China), and all other reagents were of analytical grade.

Caco-2 cells were obtained from American Type Culture Collection (USA) and cultured in RPMI-1640 medium (Corning, USA) with 1% penicillin-streptomycin (Corning, USA), and 10% fetal bovine serum (Atlanta Biologicals, USA). Cells were cultured at $37\,^{\circ}\mathrm{C}$ in a humidified incubator with 5% CO_2. Male Sprague-Dawley rats were obtained from the Experimental Animal Center of Shenyang Pharmaceutical University. All animal studies were carried out in accordance with the Guidelines for Animal Experimentation of Shenyang Pharmaceutical University and using the approved protocol by the Animal Ethics Committee of the institution.

2.2. Synthesis of L-carnitine-conjugated polymers

L-Carnitine-conjugated polymers, including L-carnitine-PEG2000-SA (stearate), L-carnitine-PEG1000-SA, L-carnitine-PEG500-SA, and L-carnitine-stearate, were synthesized using published methods in our previous papers (Kou et al., 2017b).

2.3. Preparation of L-carnitine-conjugated nanoparticles

We used a similar method to prepare L-carnitine-conjugated nanoparticles as published previously from our laboratory (Kou et al., 2017b). Briefly, PLGA, paclitaxel, and L-carnitine-conjugated polymer were dissolved in dichloromethane. The solution was added slowly in drops to 1% (w/v) PVA solution, and then sonicated using a probe-type sonifier in an ice bath. Once the resultant emulsion was achieved, dichloromethane was removed under reduced pressure. The nanoparticles in solution were collected by centrifugation at 13,000 rpm for 30 min and washed with double-distilled water three times. At the end of the procedure, the nanoparticles were freeze-dried. The nanoparticles were identified as BNP (bare nanoparticles without the ligand), CNP (L-carnitine-stearate modified nanoparticles without the linker), C5NP (L-carnitine-500-stearate modified nanoparticles with PEG500 as the linker), C10NP (L-carnitine-1000-stearate modified nanoparticles with PEG1000 as the linker), and C20NP (L-carnitine-2000-stearate modified nanoparticles with PEG2000 as the linker). The corresponding formulation compositions were shown in Table S1. When coumarin 6 used as a probe, nanoparticles were prepared by replacing paclitaxel with coumarin 6.

2.4. Characterization of L-carnitine-conjugated nanoparticles

2.4.1. Size and zeta potential
NanoZetasizer (NanoZetasizer, Malvern Co., UK) was used to measure the size, size distribution, and zeta potential of nanoparticles.

2.4.2. Entrapment efficiency (EE) and drug load (DL)
The paclitaxel untrapped in nanoparticles was removed by a Sephadex G50 column, and entrapped paclitaxel was

measured using high performance liquid chromatography (Hitachi, Tokyo, Japan). The entrapment efficiency and drug load were calculated as follows:

$$DL\ (\%) = (\text{weight of PTX in NPs/weight of PTX}$$
$$- \text{containing NPs}) \times 100\%;$$

$$EE\ (\%) = (\text{weight of PTX in NPs/weight of PTX in NPs}$$
$$+ \text{weight of untrapped PTX}) \times 100\%$$

2.4.3. Particle morphology
Transmission electron microscopy (TEM) (Hitachi H-600, Tokyo, Japan) was applied for the visualization of the morphology and shape of the nanoparticles. The nanoparticle solution was diluted and dropped onto a carbon-coated copper grid. when dried, a drop of 1% (w/v) phosphotungstic acid was added and dried again prior to TEM.

2.4.4. UV-Vis absorption spectrum
The prepared nanoparticles were dispersed in double-distilled water, and the concentration was equivalent to 5 μg/ml of paclitaxel. The absorption spectrum of nanoparticles from 200 nm to 600 nm was determined.

2.4.5. In vitro release
The release behavior of paclitaxel from nanoparticles was measured using a dialysis method (Lian et al., 2013). In brief, 2 ml of paclitaxel-loaded nanoparticles were placed in a dialysis bag (1 2 ~ 14 kDa cut-off) and incubated in 30 ml of PBS (pH 7.4) containing 2% Cremophor EL at 37 °C under shaking (100 rpm). At designated intervals, 2 ml of sample was taken out for HPLC analysis, and the same volume of fresh medium was added.

2.4.6. Stability
The stability of nanoparticles was estimated in PBS (pH 7.4) at room temperature. At designated intervals, the particle size and polydispersity index (PDI) were measured using NanoZetasizer.

2.5. Cytotoxicity

Methylthiazolyldiphenyl-tetrazolium bromide (MTT) assay was utilized to evaluate the cytotoxicity of blank nanoparticles. Briefly, Caco-2 cells were seeded into 96-well plate with a concentration of 5000 cells/well. After 12 h culturing for cell adhesion, the cells were treated with a series of concentration of nanoparticles for 48 h at 37 °C. After that, MTT solution (0.5 mg/mL) was put into the wells for another 4 h incubation. Remove the medium, and add 200 μL DMSO into wells to dissolve the formazan crystals. The absorption was measured by a multiplate reader.

2.6. In vitro cellular uptake assay

2.6.1. Uptake assay
Caco-2 cells were seeded in 24-well plates with a density of 1.5×10^5 cells/well. After 85–95% confluence was achieved, the cells were washed and incubated with 200 μl coumarin 6-loaded nanoparticles in NaCl uptake buffer. After 1 h, the cells were washed with ice-cold buffer and then solubilized with 500 μl lysis buffer. The uptake of coumarin 6-loaded nanoparticles was determined using a microplate reader with excitation/emission wavelengths at 466 nm/504 nm, and protein concentration was assessed by BCA kit (Thermo, USA).

Caco-2 cells were seed on 12-mm coverslips in 24-well plate with a density of 1.5×10^5 cells/well. When ~90% confluent, the cells were washed and incubated with coumarin 6-loaded nanoparticles for 1 h. After that, the cells were washed three times with ice-cold buffer, and the coverslip was placed sample-side down onto Antifade Mount with DAPI (ThermoFisher, USA) on the glass slide. The slides were kept in dark for 12 h, and then visualized using Nikon confocal microscope (Nikon, Japan); the mean fluorescence intensity was calculated using Image J.

2.6.2. Uptake assay in different buffers
OCTN2 transports L-carnitine in a Na^+-dependent manner. Therefore, the involvement of OCTN2 in drug uptake from the nanoparticles was examined by monitoring the uptake in the presence or absence of Na^+ or Cl^-. For this, a Na^+-free buffer, a Cl^--free buffer, and a NaCl buffer were used for uptake assays. In addition, the effect of an amount of excess L-carnitine (10 mM) on uptake was assessed to authenticate the substrate selectivity of the interaction between L-carnitine-conjugated nanoparticles and OCTN2.

2.6.3. Endocytosis mechanism
Various endocytosis inhibitors were used to investigate the endocytosis mechanisms of L-carnitine-conjugated nanoparticles. Caco-2 cells were pretreated with chlorpromazine (50 μM) (inhibitor of clathrin-dependent endocytosis), indomethacin (100 μM) (inhibitor of caveolin-dependent endocytosis), colchicine (10 μM) (inhibitor of macropinocytosis), and quercetin (10 μM) (inhibitor of caveolae- and clathrin-independent endocytosis) respectively for 30 min. The rest of steps in the handling of the cells were the same as those used in the uptake assay.

2.7. Absorption of nanoparticles in the intestinal tract

2.7.1. In situ single-pass intestinal perfusion of paclitaxel-loaded nanoparticles in rats
Rats were fasted overnight before the perfusion experiments but had free access to water. After anesthetization, the rats were depilated at the abdominal region, and a midline incision was made. A 10-cm segment of the intestinal tract (duodenum, jejunum, ileum, or colon) was exposed and the lumen of the segment was washed using 37 °C saline solution to get rid of the intestinal contents. The segment was

then tied on both ends and the resultant intestinal loop was infused with nanoparticles (10 µg/mL of paclitaxel) at a given rate. Perfusates were collected at the times indicated and the samples were used for determination of paclitaxel using HPLC. The absorption rate (Ka) and apparent permeability (P_{app}) of paclitaxel-loaded nanoparticles were calculated as described previously (Kou et al., 2017b).

2.7.2. In vivo *absorption of coumarin 6-labeled nanoparticles in the intestinal tract of rats*

Rats were fasted overnight before the experiments but had free access to water. Coumarin 6-loaded nanoparticles were orally administrated to rats (2 mg/kg). After 45 min, the rats were sacrificed, and the selected intestinal loop, about 1 cm in length, was removed, everted, cleaned, and frozen in cryoembedding media at −80 °C for 24 h. After that, the frozen intestinal loops were sectioned and fixed on slides. The tissue on slides was stained with rhodamine-phalloidin and DAPI. Finally, the slides were mounted and visualized via confocal laser scanning microscope (Nikon, Japan).

2.8. In vivo *pharmacokinetics*

Rats were fasted overnight but had free access to water and then were randomly assigned to five groups. Paclitaxel-loaded nanoparticles (10 mg/Kg) were administrated orally. Blood samples were collected at the scheduled time intervals, and the plasma fraction was separated using centrifugation for subsequent LC-MS-MS (UPLC–MS/MS, ACQUITY UPLC/tandem quadrupole detector (TQD), MassLynx V4.1 software, Waters, USA) analysis (Kou et al., 2017b). A liquid–liquid extraction by anhydrous ether was used, and docetaxel was selected as internal standard. Briefly, 100 µL of plasma was taken to mix with 100 µL of docetaxel solution and mobile phase and vortexed for 2 min. After adding 3 mL anhydrous ether, the solution was vortexed for another 3 min. Then, the mixed solution was centrifuged at 3500 rpm for 10 min, and the organic phase was collected and dried at 37 °C under a nitrogen stream. The residue was dissolved in 100 µL of Mobile phase and centrifuged 10000 rpm for 10 min, and the supernatant was taken for analysis. A positive ESI mode was selected, and quantification was carried out with m/z transitions from 854.8 to 286.2 for paclitaxel and 830.65 to 304.35 for docetaxel, respectively. The during the range of 1–2,000 ng/mL, the standard curves were linear ($r^2 \geq 0.99$), and the low limit of quantification is 1 ng/mL. The area under curve (AUC) was calculated using the trapezoidal method rule up to the last data point, and the C_{max} and t_{max} were directly read according to the curves. The terminal four points in plasma concentration-time curve were used to calculate the elimination rate constant (k), and the half-life ($t_{1/2}$) was calculated by 0.693/k.

2.9. Mucus permeation assay

A reported transwell method was used to measure the permeability of nanoparticles (Guo et al., 2019). In brief, uniform intestinal mucus (100 µL) was placed onto Transwell® 3415 chamber (Corning, NY, USA). The mucus here was obtained by slightly and carefully scraping the mucosal surfaces of the jejunum and ileum of the fasted rats. 600 µL of PBS (pH 7.4) was put into the acceptor room. After 10 min of equilibration, 200 µL of nanoparticle solution (15 µg/mL) was gently put onto the donor room. The transwell chamber was kept in an incubator at 37 °C. 200 µL of sample was taken from the receiving compartment for analysis, and same volume of PBS was placed back. The sample was diluted with acetonitrile, and the concentration of coumarin 6 was determined using a microplate reader with excitation/emission wavelengths at 466 nm/504 nm. The Papp was calculated as follows:

$$Papp = \frac{dQ}{dt} \times \frac{1}{A \times C_0}$$

dQ/dt is the permeation speed of coumarin 6 from donor room to acceptor room; A is the membrane area; C_0 is the start concentration at the donor room.

2.10. Statistical analysis

All results were shown as mean ± SD. A two-tailed Student's *t*-test was applied to assess the statistical significance of the experiments.

3. Results and discussions

3.1. Preparation and characterization of L-carnitine-conjugated nanoparticles

L-Carnitine-conjugated nanoparticles were prepared by the solvent extraction/evaporation method as described previously (Kou et al., 2017b). Based on the polyethylene glycol (PEG) linker, nanoparticles were classified as BNP (bare nanoparticles without L-carnitine modification), CNP (L-carnitine modified nanoparticles without PEG linker), C5NP (L-carnitine modified nanoparticles with PEG500 as a linker), C10NP (L-carnitine modified nanoparticles with PEG1000 as a linker), and C20NP (L-carnitine modified nanoparticles with PEG2000 as a linker). The size of all the nanoparticles was around 180 nm, and their low value of polydispersity index (PDI) corroborate the narrow size distribution (Table 1 and Figure 1(A)). This was also confirmed by the TEM (transmission electron microscope) images (shown in Figure 1(A,E–H)). The surface potential of nanoparticles was around 0 mV. Their entrapment efficiency (EE) for paclitaxel was above 70%, and the drug load (DL) was more than 3%. The absorption peak of paclitaxel, as assessed by UV-VIS spectroscopy, was around

Table 1. Characterization of L-carnitine-conjugated nanoparticles.

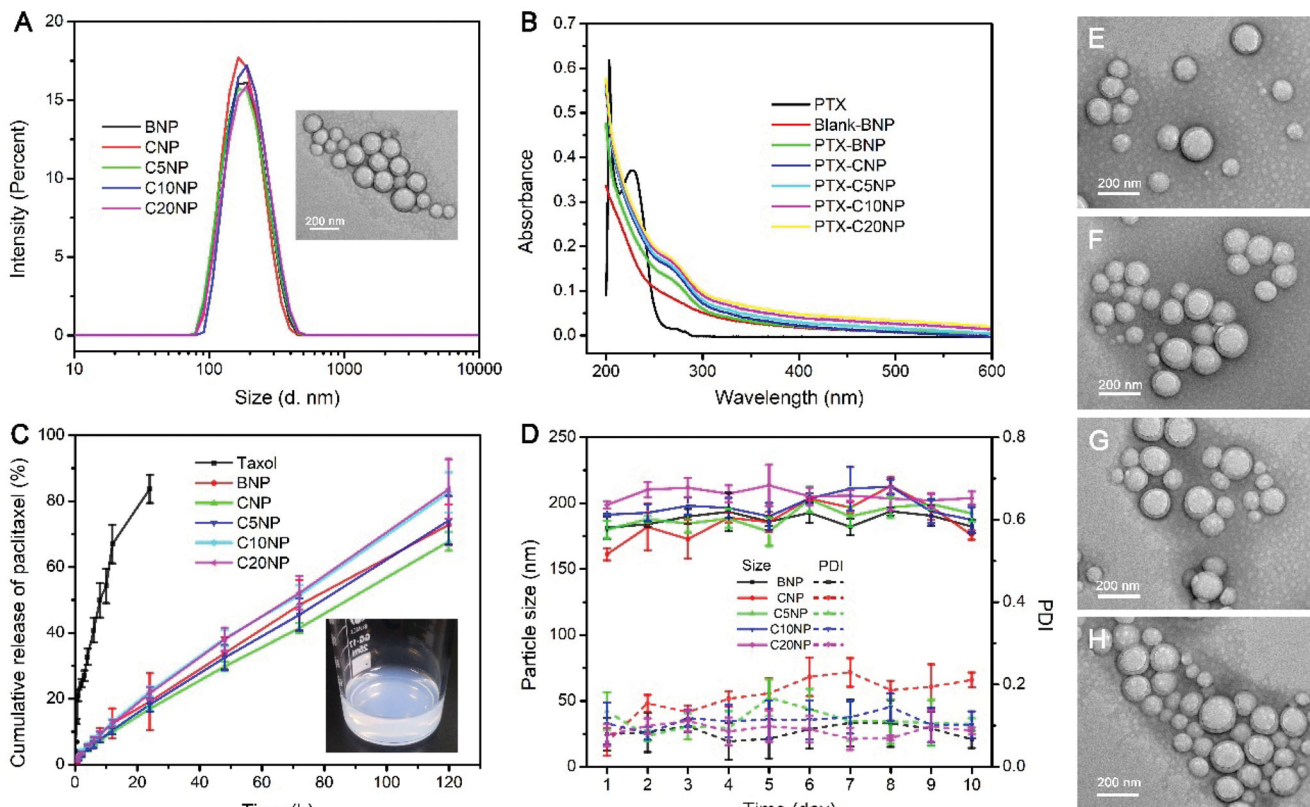| Nanoparticles	Size (nm)	PDI	Zeta potential (mV)	EE (%)	DL (%)
BNP	171.3 ± 2.0	0.065 ± 0.037	−2.38 ± 0.57	85.9 ± 4.3	4.09 ± 0.20
CNP	163.1 ± 1.9	0.154 ± 0.021	1.47 ± 0.64	73.2 ± 2.9	3.49 ± 0.14
C5NP	173.7 ± 1.2	0.075 ± 0.013	−1.53 ± 0.38	83.8 ± 3.9	3.99 ± 0.19
C10NP	176.6 ± 2.3	0.081 ± 0.015	−1.89 ± 0.44	88.9 ± 5.4	4.23 ± 0.26
C20NP	187.9 ± 0.2	0.099 ± 0.019	−1.39 ± 0.33	90.9 ± 6.3	4.33 ± 0.30

Figure 1. Characterization of L-carnitine-conjugated nanoparticles. (A) The size distribution of nanoparticles monitored by DLS, and the TEM image was for BNP; (B) The absorption spectrum of paclitaxel-loaded nanoparticles under UV-VIS; (C) The release kinetics of nanoparticles in PBS (pH7.4) containing 2% Cremophor EL at 37 °C. Inset: picture showing the clear nanoparticles with light blue opalescence; (D) The change of size and PDI of nanoparticles in PBS (pH 7.4) at room temperature; (E-H) TEM images for CNP, C5NP, C10NP and C20NP, respectively.

230 nm; this peak disappeared when paclitaxel was encapsulated into nanoparticles, indicating that paclitaxel was within the core of the nanoparticles (Figure 1(B)). The in vitro release test showed that all nanoparticles exhibited a sustained release behavior compared to the free paclitaxel (Taxol) (Figure 1(C)). The stability assay in PBS (pH 7.4) at room temperature indicated that the nanoparticles were stable and did not aggregate (Figure 1(D)). The TEM images showed that all nanoparticles had a round shape (Figure 1(E–H)), and this was confirmed by DLS (dynamic light scattering technique).

3.2. Uptake features of L-carnitine-conjugated nanoparticles in caco-2 cells

The human intestinal cells line, Caco-2, was selected as an in vitro model to investigate the uptake features of L-carnitine-conjugated nanoparticles. Before uptake assay, the cytotoxicity of blank nanoparticles was accessed. As shown in Figure S1, all five formulations of nanoparticles did not show any observed cytotoxicity to Caco-2 cells, indicating the safety of these nanoparticles. Here, coumarin 6 was used as a fluorescence probe to monitor uptake efficiency of the nanoparticles in drug delivery. It was clear that BNP showed little uptake, and the uptake was significantly increased when the cells were exposed to L-carnitine-conjugated nanoparticles. When the PEG linker length was increased from 0 up to 1000, the uptake of nanoparticles increased, but

further increase in the linker length decreased the uptake as assessed by the evaluation of uptake with immunofluorescence analysis (Figure 2(A,B)). Quantification of the immunofluorescence signals also led to the same conclusion (Figure 2(C)). These data suggested that there was an optimal linker length for maximal cellular entry of L-carnitine-conjugated nanoparticles via OCTN2. A similar phenomenon has been observed in other published reports (Zabaleta et al., 2012; Smith et al., 2013). A shorter PEG linker in L-carnitine-conjugated nanoparticles might increase the flexibility and mobility of L-carnitine, thus enhancing the targeting efficiency. When the linker length is above this threshold, it might alter the physicochemical properties of the surface of the nanoparticles and also might also shield the ligand within the PEG layer, thus interfering with the interaction between the ligand and the transporter layer (Stefanick et al., 2013). Of relevance to this issue is the fact that L-carnitine is a small molecule, which could easily be masked by the increased size of the PEG linker; this might not be an issue if the ligand is a macromolecule such as antibodies.

We also evaluated the involvement of OCTN2 in the uptake of L-carnitine-conjugated nanoparticles with or without the PEG linker (CNP, C5NP, C10NP, and C20NP) by monitoring the Na^+-dependence of the uptake process. OCTN2 interacts with L-carnitine and mediates its transport in a Na^+-dependent manner. If the observed uptake of L-carnitine-conjugated nanoparticles in Caco-2 cells is obligatorily dependent on the interaction of the L-carnitine ligand on
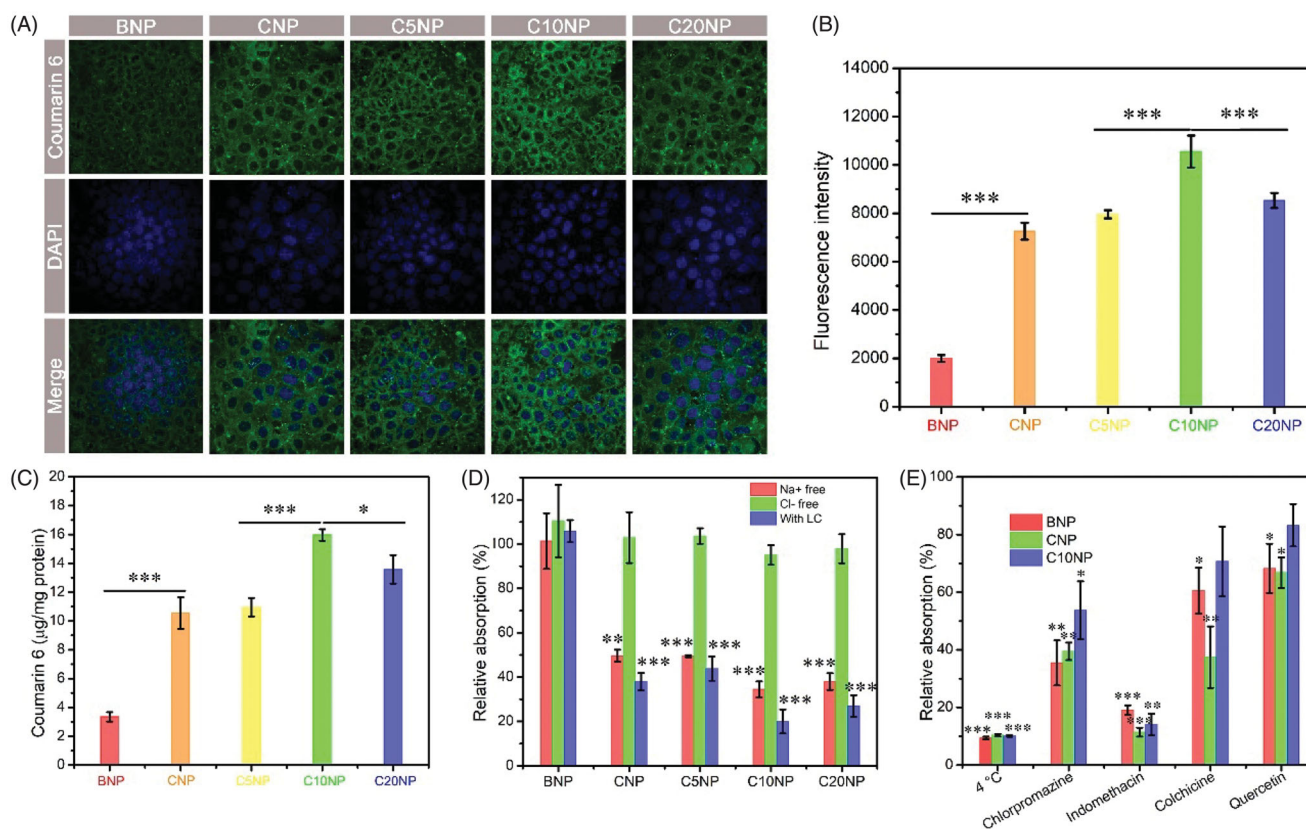
Figure 2. Uptake features of L-carnitine-conjugated nanoparticles in Caco-2 cells. (A) Confocal microscopy image of Caco-2 cells incubated with L-carnitine-conjugated nanoparticles for 1 h. Blue: DAPI for nuclei, Green: coumarin 6; (B) Quantitative analysis of the fluorescence signals in the confocal images using Image J; (C) Uptake assay of L-carnitine-conjugated nanoparticles in NaCl uptake buffer; (D) The relative absorption of nanoparticles in Na^+-free buffer, Cl^--free buffer, and NaCl buffer with excess L-carnitine (LC; 10 mM), and BNP group was used as the control; (E) Impact of endocytosis inhibitors on the uptake of nanoparticles in Caco-2 cells, and the uptake of nanoparticles without treatment was used as the control. Data are shown as mean ± SD, $n = 3$, *, $p < .05$, **, $p < .01$, ***, $p < .001$ vs control group.

the surface of the nanoparticles with OCTN2, then the uptake process is expected to be Na^+-dependent. Therefore, we examined the influence of Na^+ and Cl^- on the uptake of L-carnitine-conjugated nanoparticles (Figure 2(D)). The uptake of BNP was independent of both Na^+ and Cl^-. For L-carnitine-conjugated nanoparticles, the uptake was Na^+-dependent, but Cl^--independent. These data confirm the involvement of OCTN2 in the uptake of L-carnitine-conjugated nanoparticles.

Another feature of transporter-mediated uptake of ligand-conjugated nanoparticles is the substrate selectivity. As OCTN2 is a carnitine transporter, free carnitine should compete with the ligand L-carnitine on the surface of the nanoparticles for interaction with the transporter. Therefore, free carnitine is expected to inhibit the interaction of L-carnitine-conjugated nanoparticles and hence their uptake in Caco-2 cells. This was indeed the case. Excess free L-carnitine into the uptake buffer resulted in a significant decrease in the uptake of L-carnitine-conjugated nanoparticles (Figure 2(D)).

Because of the large size of the nanoparticles, transporter-mediated uptake of such macromolecules is not expected to occur via the routine process of simple translocation across the plasma membrane. Most published reports on this phenomenon indicates endocytosis as the mechanism of uptake. We investigated the involvement of endocytosis in OCTN2-mediated L-carnitine-conjugated nanoparticles in Caco-2 cells

using selective inhibitors of different modes of endocytosis. Coumarin 6 was used as a marker to track the uptake process. Firstly, we monitored the temperature dependence of the uptake process. At 4 °C, the uptake of BNP, CNP, C10NP was drastically decreased, suggesting involvement of a transporter in the uptake process. Different endocytosis inhibitors had different effects on uptake. Indomethacin, the inhibitor of caveolin-mediated endocytosis, showed the most potent inhibitory effect; chlorpromazine showed 50% inhibition. Colchicine (an inhibitor of macropinocytosis) and quercetin (an inhibitor of caveolin/clathrin-independent endocytosis) showed the least effect. These data indicated that caveolin-mediated endocytosis and clathrin-mediated endocytosis might play an important role in the uptake of nanoparticles. Taken collectively, these studies show that L-carnitine conjugated nanoparticles might employ OCTN2-dependent endocytosis for enhanced cellular uptake.

3.3. Intestinal absorption of L-carnitine-conjugated nanoparticles

In situ single-pass perfusion with different intestinal segments (duodenum, jejunum, ileum, and colon) was performed to determine the intestinal absorption efficiency of L-carnitine-conjugated nanoparticles. The apparent permeability (P_{app}) and the absorption rate (Ka) were measured to
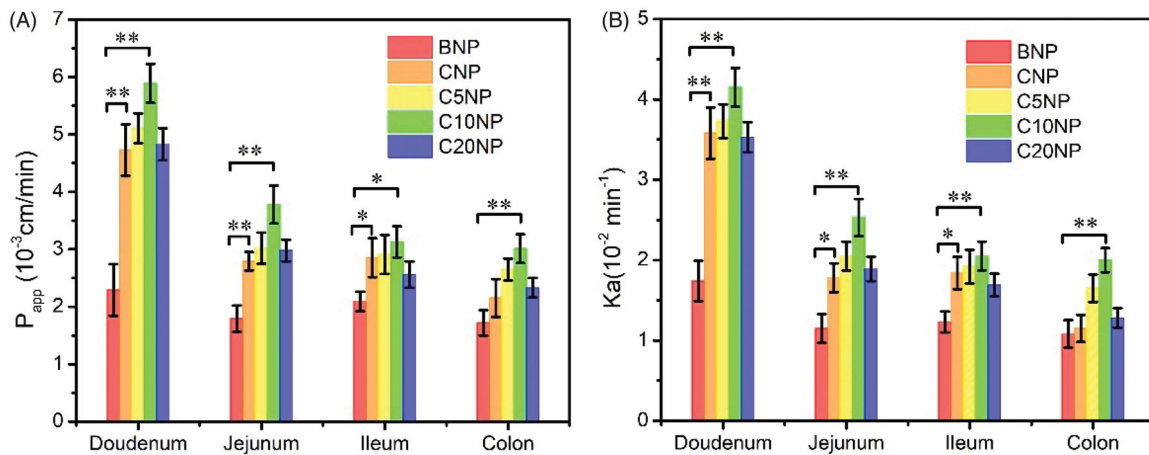
Figure 3. The apparent permeability (P_{app}) (A) and the absorption rate (Ka) (B) of BNP and L-carnitine-conjugated nanoparticles in *in situ* intestinal perfusion. Data are shown as mean ± SD, $n = 3$. *, $p < .05$; **, $p < .01$.

compare the delivery efficiency of paclitaxel-loaded nanoparticles (Figure 3). It was clear that L-carnitine-conjugated nanoparticles increased the P_{app} and Ka of paclitaxel compared to BNP in all intestinal segments studied. With the increasing length of the PEG linker from 0 to 1000, the P_{app} and Ka increased in intestinal segments representing duodenum, jejunum, ileum, and colon. Further, increase in the linker size beyond 1000, the values for P_{app} and Ka decreased. C10NP showed the highest P_{app} or Ka in all the intestinal segments. These results were consistent with the cellular uptake assay.

We then investigated the *in vivo* efficacy of L-carnitine-conjugated nanoparticles in rats. For this, we administered coumarin 6-loaded nanoparticles to the animals via the oral route. Then, the intestinal segments were taken out for absorption analysis. As shown in Figure 4, the results of these *in vivo* experiments were surprisingly very different from what we found in *in vitro* and in *in situ* experiments. The absorption *in vivo* was maximal with CNP that had no PEG linker. Of course, BNP that had no L-carnitine as the ligand showed much less absorption, indicating that the presence of the L-carnitine on the surface of the nanoparticles did enhance the absorption *in vivo*. But the facilitating effect of the PEG linker that was seen *in vitro* and *in situ* was not seen *in vivo*. In fact, the presence of the PEG linker compromised the absorption seen with CNP.

3.4. In vivo *pharmacokinetics*

In vivo pharmacokinetics was performed to further determine the impact of the PEG linker in L-carnitine-conjugated nanoparticles on intestinal absorption *in vivo*. The results are shown in Figure 5 and Table 2. The data were consistent with the results of *in vivo* intestinal absorption. When there was no linker (i.e. CNP), the oral absorption was maximal and significantly greater than BNP, C5NP, C10NP, and C20NP. This was evident both in AUC and Cmax. In fact, the presence of the PEG linker actually had a marked drastic effect on *in vivo* oral absorption as the absorption with the linker was even less than nanoparticles without the ligand.

This project was undertaken with the notion that if introduce the PEG linker between the L-carnitine ligand and the surface of the nanoparticles, it would increase the flexibility and mobility of the conjugated ligand for increased targeting efficiency of nanoparticles and to increase the permeability of nanoparticles across the mucus layer as has been shown in other cases (Song et al., 2018). The results of the *in vitro* and *in situ* experiments did support this notion; upto a point, the longer was the PEG linker, the more efficient the uptake of the nanoparticles in Caco-2 cells (*in vitro*) and intestinal segment perfusion (*in situ*). There was however an optimal length of the linker (PEG1000) as any further increase in the length compromised the uptake. This is understandable because the ligand could be masked within the linker if it is too long, thereby making it difficult for the ligand to be accessible to the transporter for interaction. But, what was surprising was that the *in vitro* and *in situ* data were not corroborated by *in vivo* data. In intact animals with oral administration of the nanoparticles, the addition of the PEG linker did not improve the efficiency of intestinal absorption nor did it improve the pharmacokinetic profile. In fact, the addition of the linker interfered with the absorption. Nonetheless, the *in vivo* experiments do support unequivocally the idea that the addition of the L-carnitine ligand to the surface of the nanoparticles facilitates the targeting to the carnitine transporter OCTN2.

What could be the explanation for the difference between the *in vitro/in vivo* data and the *in vivo* data? We speculate that the presence of the intact mucus layer *in vivo*, which is absent *in vitro* and *in situ* experiments, could be the reason for the difference. In *in situ* intestinal perfusion experiment, the intestinal lumen was rinsed many times to remove the feces and to equilibrate the experimental condition, probably leading to a significantly reduced thickness of the mucus layer. Thus, the *in situ* intestinal perfusion data were more consistent with the *in vitro* data, but they differ from the *in vivo* data. When crossing the mucus layer, the diffusion rate of BNP would be slow due to the hydrophobic surface. CNP has a comparatively more hydrophilic surface because of L-carnitine modification, which might increase the diffusion rate. When the PEG linker was inserted, the
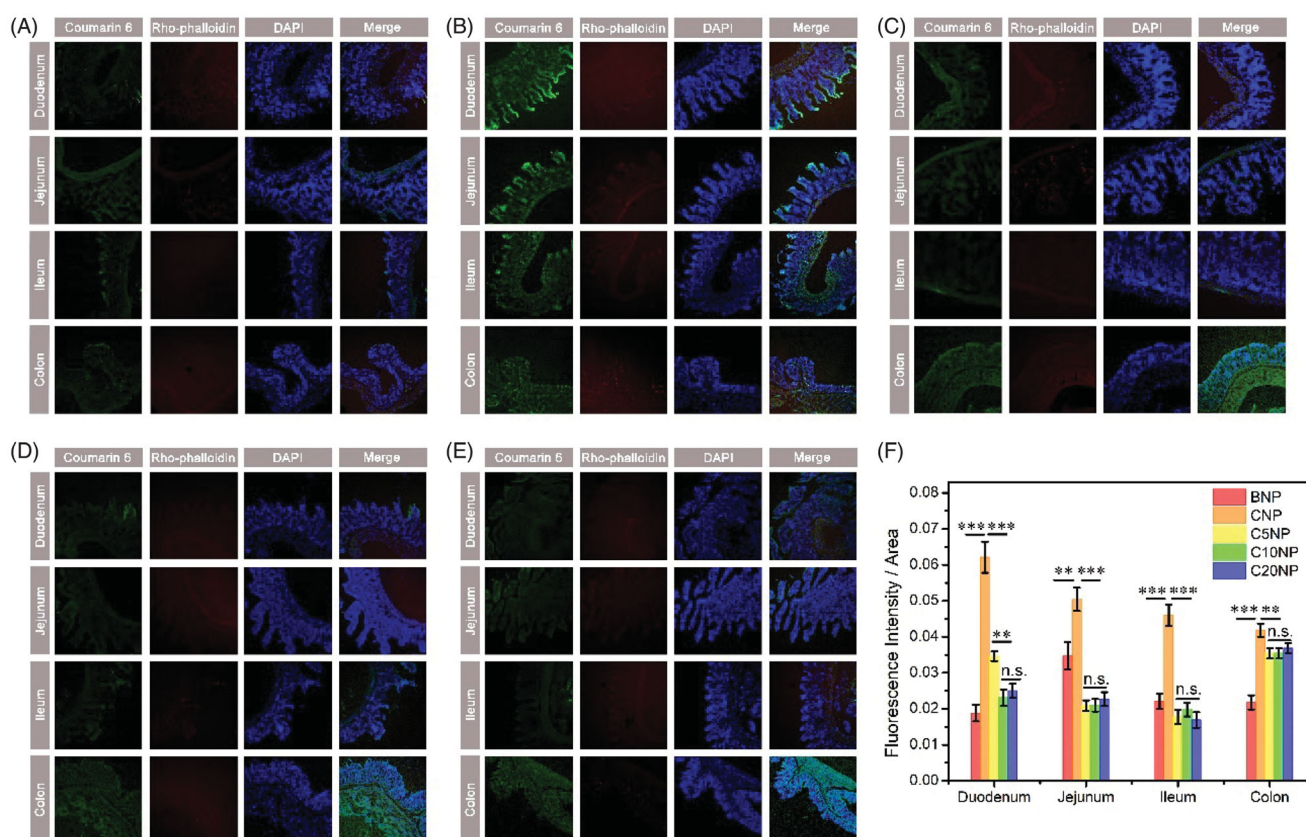
Figure 4. The fluorescence images of rat intestinal sections after oral administration of coumarin 6-loaded (A) BNP, (B) CNP, (C) C5NP, (D) C10NP, and (E) C20NP; (F) Quantitative analysis of the fluorescence signals using Image J. Blue: DAPI for nuclei, Green: coumarin 6-labeled nanoparticles, Red: rhodamine phalloidin for cytoskeleton. Data are shown as mean ± SD, $n = 3$. *, $p < .05$; **, $p < .01$; ***, $p < .001$.
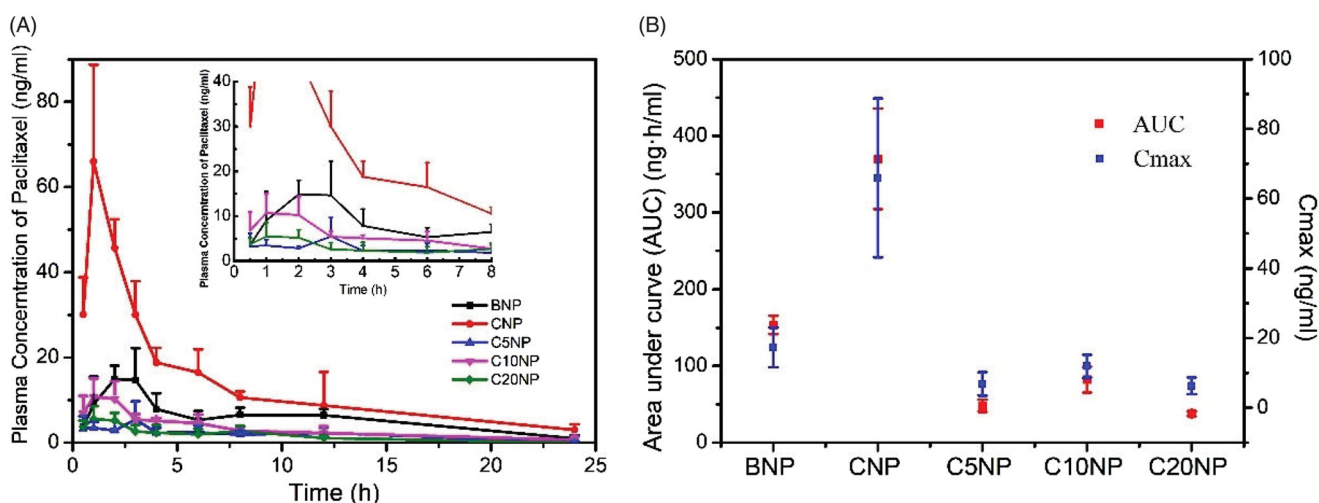

Figure 5. Pharmacokinetic profiles of paclitaxel in rats after oral administration. (A) Plasma levels of paclitaxel following oral administration of L-carnitine-conjugated nanoparticles; (B) AUC and Cmax of the pharmacokinetic profiles of paclitaxel loaded in nanoparticles. Date is given as means ± SD, $n = 6$.

Table 2. Pharmacokinetic parameters of paclitaxel after oral administration of L-carnitine-conjugated nanoparticles in rats (Mean ± SD, $n = 6$).

	Cmax (ng/ml)	Tmax (h)	AUC$_{(0-24)}$ (ng·h/ml)	$T_{1/2}$ (h)	F_R^α (%)
BNP	17.34 ± 5.70	2.00 ± 0.82	153.70 ± 12.03	10.63 ± 3.41	100
CNP	65.95 ± 22.79**	1.00 ± 0	369.99 ± 65.65**	12.43 ± 3.94	241
C5NP	6.87 ± 3.37**	2.13 ± 1.65	48.26 ± 7.98**	9.38 ± 2.32	31
C10NP	11.94 ± 3.30*	1.38 ± 0.65	82.09 ± 16.85**	7.37 ± 2.09	53
C20NP	6.32 ± 2.40**	1.50 ± 0.85	37.70 ± 3.06**	4.32 ± 2.34	25

$^\alpha F_R$ is the relative oral bioavailability compared to BNP; *$p < .05$, **$p < .01$ versus BNP group.

hydrophilicity was supposed to facilitate the diffusion rate (Inchaurraga et al., 2015), but it was not the case. The addition of the PEG linker most likely leads to trapping of the positively charged L-carnitine ligand within the negatively charged mucus layer because of the increased flexibility of the ligand in the presence of the linker. This idea is depicted schematically in Figure 6. To further confirm that, a permeation assay using mucus layer covered donor-acceptor compartments was performed. As shown in Figure S3(A,B), the
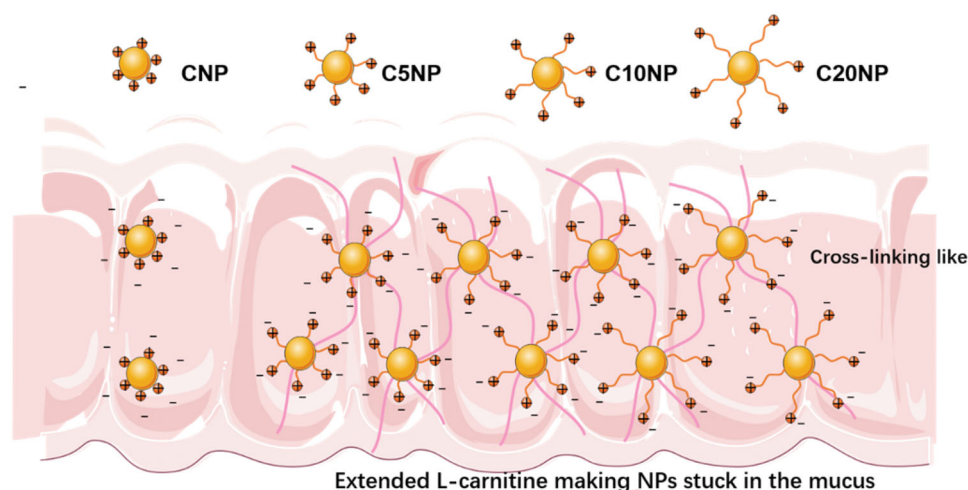
Figure 6. A schematic model for the detrimental effect of the PEG linker on oral absorption of L-carnitine-conjugated nanoparticles *in vivo*.

cumulative permeation of nanoparticles through the mucus layers was linearly increased over time. The Papp value of CNP was significantly higher than those of BNP, C5NP, C10NP, and C20NP. These results were in support of our hypothesis. Otherwise, the inserted PEG also has the capability to influence the activity of some transporters, and even consume energy, might also contributing the compromised performance of L-carnitine conjugated nanoparticles with PEG linkers (Thakkar & Desai, 2015; Kou et al., 2018c). Obviously, additional studies are needed to understand why the PEG linker has negative impact on oral absorption of the L-carnitine-conjugated nanoparticles *in vivo*.

4. Conclusion

We developed L-carnitine-conjugated nanoparticles with an idea of improving oral bioavailability of therapeutic drugs by targeting the intestinal carnitine transporter OCTN2. The results of the experiments with these L-carnitine-conjugated nanoparticles are encouraging in that the addition of L-carnitine as the ligand did enhance absorption of drugs entrapped in the nanoparticles *in vitro* (Caco-2 cells), *in situ* (isolated intestinal segment perfusion), and *in vivo* (intact animals). However, the idea that addition of a PEG linker between the ligand and the nanoparticle surface would further enhance the uptake of the nanoparticles in intestinal cells did not turn out to be true.

Disclosure statement

The authors declare no conflict of interest.

References

Chacko A-M, Nayak M, Greineder CF, et al. (2012). Collaborative enhancement of antibody binding to distinct PECAM-1 epitopes modulates endothelial targeting. Plos One 7:e34958.

Chu C, Xu P, Zhao H, et al. (2016). Effect of surface ligand density on cytotoxicity and pharmacokinetic profile of docetaxel loaded liposomes. Asian J Pharm Sci 11:655–61.

Date AA, Hanes J, Ensign LM. (2016). Nanoparticles for oral delivery: design, evaluation and state-of-the-art. J Control Release 240:504–26.

Giacomini KM, Huang S-M, Tweedie DJ, International Transporter Consortium, et al. (2010). Membrane transporters in drug development. Nat Rev Drug Discov 9:215–36.

Guo M, Wei M, Li W, et al. (2019). Impacts of particle shapes on the oral delivery of drug nanocrystals: mucus permeation, transepithelial transport and bioavailability. J Control Release 307:64–75.

Howard M, Zern BJ, Anselmo AC, et al. (2014). Vascular targeting of nanocarriers: perplexing aspects of the seemingly straightforward paradigm. Acs Nano 8:4100–32.

Hu C, Tao L, Cao X, et al. (2019). The solute carrier transporters and the brain: physiological and pharmacological implications. Asian J Pharm Sci. doi:10.1016/j.ajps.2019.09.002.

Inchaurraga L, Martín-Arbella N, Zabaleta V, et al. (2015). *In vivo* study of the mucus-permeating properties of PEG-coated nanoparticles following oral administration. Eur J Pharm Biopharm 97:280–9.

Kennedy D, Leibach FH, Ganapathy V, et al. (2002). Optimal absorptive transport of the dipeptide glycylsarcosine is dependent on functional Na+/H + exchange activity. Pflügers Archiv 445:139–46.

Kharya P, Jain A, Gulbake A, et al. (2013). Phenylalanine-coupled solid lipid nanoparticles for brain tumor targeting. J Nanopart Res 15:1–12.

Kou L, Bhutia YD, Yao Q, et al. (2018a). Transporter-guided delivery of nanoparticles to improve drug permeation across cellular barriers and drug exposure to selective cell types. Front Pharmacol 9:27.

Kou L, Hou Y, Yao Q, et al. (2017a). L-Carnitine-conjugated nanoparticles to promote permeation across blood–brain barrier and to target glioma cells for drug delivery via the novel organic cation/carnitine transporter OCTN2. Artif Cell Nanomed Biotechnol 46:1605–1616.

Kou L, Jiang X, Xiao S, et al. (2019). Therapeutic options and drug delivery strategies for the prevention of intrauterine adhesions. J Control Release 318:25–37.

Kou L, Sun J, Zhai Y, et al. (2013). The endocytosis and intracellular fate of nanomedicines: implication for rational design. Asian J Pharm Sci 8:1–10.

Kou L, Sun R, Bhutia YD, et al. (2018b). Emerging advances in P-glycoprotein inhibitory nanomaterials for drug delivery. Expert Opin Drug Deliv 15:869–79.

Kou L, Sun R, Ganapathy V, et al. (2018c). Recent advances in drug delivery via the organic cation/carnitine transporter 2 (OCTN2/SLC22A5). Expert Opin Ther Targets 22:715–26.

Kou L, Yao Q, Sivaprakasam S, et al. (2017b). Dual targeting of l-carnitine-conjugated nanoparticles to OCTN2 and ATB0+ to deliver chemotherapeutic agents for colon cancer therapy. Drug Deliv 24: 1338–49.

Kou L, Yao Q, Sun M, et al. (2017c). Cotransporting ion is a trigger for cellular endocytosis of transporter-targeting nanoparticles: a case study of high-efficiency SLC22A5 (OCTN2)-mediated carnitine-conjugated nanoparticles for oral delivery of therapeutic drugs. Adv Healthcare Mater 6:1700165.

Li L, Di X, Wu M, et al. (2017). Targeting tumor highly-expressed LAT1 transporter with amino acid-modified nanoparticles: toward a novel active targeting strategy in breast cancer therapy. Nanomedicine 13: 987–98.

Lian H, Zhang T, Sun J, et al. (2013). Enhanced oral delivery of paclitaxel using acetylcysteine functionalized chitosan-vitamin E succinate nanomicelles based on a mucus bioadhesion and penetration mechanism. Mol Pharmaceutics 10:3447–58.

Luo Q, Gong P, Sun M, et al. (2016). Transporter occluded-state conformation-induced endocytosis: amino acid transporter ATB 0,+-mediated tumor targeting of liposomes for docetaxel delivery for hepatocarcinoma therapy. J Control Release 243:370–80.

Qing Y, Longfa K, Ying T, et al. (2018). MMP-responsive 'smart' drug delivery and tumor targeting. Trends Pharmacol Sci 39:766–81.

Regina-Veronicka K, et al. (2018). Recent advances in "smart" delivery systems for extended drug release in cancer therapy. Int J Nanomed 13:4727–45.

Shao K, Ding N, Huang S, et al. (2014). Smart nanodevice combined tumor-specific vector with cellular microenvironment-triggered property for highly effective antiglioma therapy. ACS Nano 8:1191–203.

Smith CA, Simpson CA, Kim G, et al. (2013). Gastrointestinal bioavailability of 2.0 nm diameter gold nanoparticles. Acs Nano 7:3991–6.

Song W, Yang Y, Yu M, et al. (2018). Enhanced digestion inhibition and mucus penetration of F127-modified self-nanoemulsions for improved oral delivery. Asian J Pharm Sci 13:326–35.

Stefanick JF, Ashley JD, Kiziltepe T, et al. (2013). A systematic analysis of peptide linker length and liposomal polyethylene glycol coating on cellular uptake of peptide-targeted liposomes. Acs Nano 7:2935–47.

Thakkar H, Desai J. (2015). Influence of excipients on drug absorption via modulation of intestinal transporters activity. Asian J Pharm 9:69.

Wang Z, Guo W, Kuang X, et al. (2017). Nanopreparations for mitochondria targeting drug delivery system: current strategies and future prospective. Asian J Pharm Sci 12:498–508.

Yao Q, Choi JH, Dai Z, et al. (2017a). Improving tumor specificity and anticancer activity of dasatinib by dual-targeted polymeric micelles. Acs Appl Mater Interfaces 9:36642–36654.

Yao Q, Dai Z, Choi JH, et al. (2017b). Building stable MMP2-responsive multifunctional polymeric micelles by an all-in-one polymer-lipid conjugate for tumor-targeted intracellular drug delivery. Acs Appl Mater Interfaces 9:32520–32533.

Yao Q, Gutierrez DC, Hoang NH, et al. (2017c). Efficient co-delivery of paclitaxel and curcumin by novel bottlebrush copolymer-based micelles. Mol Pharm 14:2378–2389.

Yao Q, Liu Y, Kou L, et al. (2019). Tumor-targeted drug delivery and sensitization by MMP2-responsive polymeric micelles. Nanomedicine 19: 71–80.

Zabaleta V, Ponchel G, Salman H, et al. (2012). Oral administration of paclitaxel with pegylated poly(anhydride) nanoparticles: permeability and pharmacokinetic study. Eur J Pharm Biopharm 81:514–23.